HHS Public Access

Author manuscript

J Orthop Res. Author manuscript; available in PMC 2015 July 01.

Published in final edited form as:

J Orthop Res. 2014 July ; 32(7): 880–886. doi:10.1002/jor.22620.

ENDPLATE DEFLECTION IS A DEFINING FEATURE OF VERTEBRAL FRACTURE AND IS ASSOCIATED WITH PROPERTIES OF THE UNDERLYING TRABECULAR BONE

Timothy M Jackman[1], **Amira I Hussein**[2], **Alexander M Adams**[1,2], **Kamil K Makhnejia**[1], and **Elise F Morgan**[1,2]

[1] Dept. of Biomedical Engineering, Boston University, Boston, MA, United States

[2] Dept. of Mechanical Engineering, Boston University, Boston, MA, United States

Abstract

Endplate deflection frequently occurs with vertebral failure, but the relationship between the two remains poorly defined. This study examined associations between endplate deflection under compressive loading and characteristics of the neighboring subchondral bone and intervertebral disc (IVD). Ten L1 vertebrae with adjacent IVDs were dissected, compressed axially in a stepwise manner to failure, and imaged with micro-computed tomography before each loading step. From the images, deflection was measured across the surface of each endplate at each step. Trabecular microstructure and endplate volume fraction were evaluated in 5mm regions just under the superior endplate. IVDs were assessed using computed tomography and histology. A marked increase in superior endplate deflection coincided with a drop in the load-displacement curve. Endplate deflection was higher in regions with less robust bone microstructure ($p<0.009$), though these associations tended to weaken as loading progressed. Immediately following the ultimate point, endplate deflection was higher in regions underlying the nucleus pulposus vs. annulus fibrosus ($p=0.035$), irrespective of disc grade ($p=0.346$). These results indicate that a sudden increase in endplate deflection signals that the mechanical competence of the vertebra has been compromised. The mechanisms of endplate failure likely relate to anatomical features of the endplate, neighboring trabecular bone, and IVD.

Keywords

vertebral fracture; vertebral endplate; intervertebral disc; cancellous bone; spine biomechanics

INTRODUCTION

Vertebral fractures affect at least 12-20% of men and women over the age of 50 years,[1-3] and the risk of fracture increases exponentially with age.[4] These osteoporotic fractures are notable for their high associated morbidity[5] and increased risk of death.[6] Vertebral fracture is a strong predictor of future fractures in the spine, hip, and wrist, even after adjusting for

Timothy M. Jackman, Department of Biomedical Engineering, Boston University, 44 Cummington Mall, Boston, MA 02215, Phone: 617-358-3419, Fax: 617-353-5866, jackmant@bu.edu.

bone mineral density.[7-9] Understanding the mechanisms of vertebral failure will likely have extensive clinical impact with respect to prevention and treatment of fractures in the aging population. Some clinical classifications[10-12] of vertebral fractures and deformities associate large endplate deflection with vertebral failure, indicating that the endplates may play a critical role in mechanical failure of the vertebra.

Biomechanical studies[13-16] of vertebral fractures have reported large endplate deflection in conjunction with vertebral failure, but the precise relationship remains poorly defined. Specifically, whether vertebral failure initiates with endplate deflection is not clear at present. Initial endplate injury in motion segments has been observed to coincide with a decrease in stiffness prior to failure,[17] and excessive endplate bulging and trabecular collapse have been reported to accompany endplate fractures.[13,14,18] The underlying trabecular bone is widely agreed to provide mechanical support to the endplate: near the endplate, the subchondral trabecular bone, and not the cortical shell, bears almost the entire load supported by the vertebral body.[19,20] Regional variations in microstructure, stiffness, and strength have been observed in the underlying trabecular bone,[21-23] and these properties also change with age and the development of osteoporosis.[24] Such variations in the mechanical behavior of the adjacent bone may affect both the initiation and progression of endplate deflection and, by extension, vertebral failure.

Degeneration of the adjacent intervertebral disc (IVD) may also influence endplate deflection. In axial compression, healthy IVDs maintain approximately uniform pressure across the nucleus pulposus (NP), but in degenerated IVDs, the regions of high pressure shift to the annulus fibrosus (AF).[25,26] This shift reduces the load borne by the trabecular core,[27] and may reduce in-plane tensile strains in the central endplate.[28] When compared to motion segments with healthy IVDs, those with degenerated IVDs exhibit less spatial variation in stiffness of the neighboring bone.[29] These studies demonstrate that IVD degeneration alters the loading profile across the endplate and suggest that the underlying trabecular bone may adapt to the new mechanical environment. Thus, IVD health may play a role in the mechanisms of vertebral failure, via effects on vertebral loading and/or trabecular microstructure.

The overall goal of this study was to investigate the relationship between endplate deflection and vertebral failure, with emphasis on associations between endplate deflection and characteristics of the neighboring subchondral bone and IVD. The objectives were: 1) to quantify axial deflection of the endplate using a series of micro-computed tomography (μCT) images acquired as the vertebra was compressed to failure; 2) to identify associations between endplate deflection and the microstructure of the endplate and subchondral trabecular bone; and 3) to examine the role of IVD health in endplate deflection.

METHODS

Specimen Preparation

Ten functional spine units, each consisting of the L1 vertebra with adjacent IVDs and adjoining endplates of T12 and L2, were dissected from fresh-frozen human spines (age: 61-88 years; 5 male, 5 female; NDRI, Philadelphia, PA) by making transverse cuts just

above the inferior endplate of T12 and below the superior endplate of L2. The posterior elements were removed due to the size constraints of the μCT scanner. The specimens were kept hydrated and, when not in use, wrapped in saline-soaked gauze, sealed in plastic bags, and stored at −20°C.

Mechanical Testing and Imaging

The top and bottom surfaces of the specimens were potted in circular dishes filled with polymethyl methacrylate (PMMA). Each specimen was first imaged with quantitative computed tomography (QCT; GE Lightspeed VCT; GE Healthcare, Milwaukee, WI; 0.32×0.32×0.626 mm/voxel) and then placed in a custom-built, radiolucent device for mechanical testing (Figure 1). After ten cycles of preconditioning to 400N, the specimens were imaged with μCT (μCT 80, Scanco Medical, Brüttisellen, Switzerland; 37 μm/voxel). The settings for voltage, current and integration time were 70 kVp, 114 mA, and 300 ms, respectively. Scan times ranged 3.5-4.0 hours. Each specimen was then axially compressed in a stepwise manner (1 mm/step, rate: 0.25 mm/s) by turning the top screw cap to apply the specified displacement.[30] After a 20-minute relaxation period, the loaded specimen underwent another μCT scan, with the same scan settings. This stepwise loading was continued to failure, defined as the specimen's ultimate point. The specimen was then unloaded and imaged with μCT to quantify any post-loading recovery.

Endplate Deflection

Image registration (IPL; Scanco Medical) was used to align the series of images of the entire vertebral body. The minimum acceptable correlation coefficient between pairs of registered images was set at 0.8; visual inspection was also performed to ensure the images were properly aligned. The surfaces of the calcified endplates of L1 were determined from the aligned images using a semi-automated, custom algorithm in MATLAB (MathWorks, Inc., Natick, MA). This algorithm used a Gaussian filter (sigma: 1, support: 2) and a global threshold to identify the boundary between calcified and cartilaginous endplate. The threshold, 15% of the maximum grayscale intensity (or 4915 on a 16-bit scale), was selected based on an adaptive, iterative technique (Scanco Medical) for segmentation of bone tissue from marrow. Endplate deflection, defined as the change in axial position between the aligned images, was measured at each pixel on the calcified endplate surface at each load increment (Figure 2). The three load increments that immediately followed clear initiation of endplate deflection, defined as deflection exceeding 0.2 mm anywhere on the endplate surface, were identified. This 0.2mm threshold was chosen based on considerations of the measurement precision of endplate deflection.

Subchondral Trabecular Microstructure and Endplate Volume Fraction

A grid of contiguous, 5mm squares was defined just under the superior endplate. Each square defined the sides of a 3-D volume of interest (VOI) that extended from the inferior aspect of the endplate down to a depth of 5 mm (Figure 3). Apparent density (ρ_{app}), volume fraction, trabecular separation (Tb.Sp*), trabecular number (Tb.N*), connectivity density (ConnD), degree of anisotropy (DA), structural model index (SMI), and mean deflection were evaluated for each VOI. The same grid of 5mm squares, but with a VOI depth of 2 mm that started from the superior aspect of the endplate,[31] was used for computation of volume

fraction, termed as endplate volume fraction (Ep.BV/TV). All analyses used a Gaussian filter (sigma = 0.8; support = 1) and threshold of 4915.

IVD Histology and Grading

Histological assessment (supplementary material: S1) of the T12-L1 IVDs was performed to identify the location of the NP and to evaluate the overall health of the disc. The IVDs were also graded from photographs taken during extraction[32] and from the QCT images, the latter according to the grading scale, "apparent loss of disc integrity" ("ALDI"; supplementary material: S2)[33], which ranges from 0 (no/mild degeneration) to 2 (severe degeneration) (Figure 4). With the severely degenerated IVDs (n = 3), the NP boundary was not visible in the QCT images and was instead approximated according to Adams et al.[25] (supplementary material: S3). The subchondral VOIs were identified as underlying either the NP or AF.

Statistical Analyses

For each parameter of bone microstructure, a repeated-measures analysis of variance (ANOVA) (JMP 9.0, SAS Institute Inc., Cary, NC) was carried out with load increment as the within-subjects factor and the microstructural parameter as a between-subjects factor. An additional factor, the distance of the VOI to the site of initial deflection ("VOI distance"; Figure 5), was included in the ANOVA model, to control for the distance when evaluating the association between deflection and microstructure (*i.e.* to account for the possibility that large deflection would be more likely in regions close to the site of initial deflection). An ANOVA was performed for each load increment individually, as a *post-hoc* test to determine how the association between trabecular microstructure and endplate deflection changed as loading progressed. A paired *t*-test with ALDI score as the grouping variable was used to compare median deflection in the region of endplate adjacent to the NP and AF at the single increment just after the ultimate point. A significance level of 0.05 was used for all statistical analyses.

RESULTS

The superior endplates exhibited a marked increase in deflection that coincided with a drop in the load-displacement curve (Figure 6, Table 1). The average (± standard deviation) maximum deflection of the superior endplate was 0.91 (± 0.60) mm prior to the drop in load and then increased 1.22 mm on average (Figure 7, Table 2). Circumferential cracks appeared in six of the ten superior endplates. Eight failed in the posterior half—and specifically in the ring apophysis for five of these eight—while two failed in the anterior half. On average, 68% (±18%) of the maximum deflection at the last loading increment remained in the superior endplate after unloading. Deflection of the inferior endplates never exceeded 0.15 mm at any load increment.

Irrespective of VOI distance and for all load increments, endplate deflection was higher in regions with high Tb.Sp*, SMI (Figure 8A), and DA ($p<0.001$) and lower in regions with high Tb.N*, ConnD, and Ep.BV/TV (Figure 8B) ($p<0.009$), though substantial variations were observed among specimens. An effect of load increment was observed ($p<0.034$) in that the aforementioned associations tended to weaken as loading progressed. VOIs with

higher ρ_{app} experienced smaller deflections (p=0.003) at the first of the three increments; no correlation was found in the other two increments (p>0.324). For the increment corresponding to the large drop in the load-displacement curve, the median endplate deflection in the NP region was higher than that in the AF region (0.46 mm vs. 0.21 mm, p=0.035), irrespective of disc grade (p=0.346).

DISCUSSION

With both clinical classifications[10-12] and biomechanical studies[13-16] identifying endplate deflection as a frequent feature of vertebral fractures and deformities, our goal in this study was to examine the relationship between endplate deflection and vertebral failure. Further, to understand the mechanisms underlying this relationship, we investigated associations between endplate deflection and structural properties of the endplate, adjacent bone and IVD. We found that sudden and non-recoverable endplate deflection was a defining feature of biomechanical failure of the vertebra. Although large endplate deflection was initially localized, a marked increase in endplate deflection indicated that the mechanical competence of the vertebra had been severely compromised. Endplate deflection initially propagated preferentially to regions of lower Ep.BV/TV and less robust trabecular microstructure, and these associations with bone microstructure then waned as loading progressed. Immediately after the point of vertebral failure (the ultimate point), deflection was larger in regions adjoining the NP, for all IVD grades. These results connote a biomechanical basis for clinical use of large endplate deflection as a characteristic of vertebral deformities and fracture,[10-12] and they suggest that the failure mechanisms relate to anatomical features of the endplate, neighboring bone, and IVD.

A novel aspect of this study is that it examined both the initiation and propagation of endplate deflection using quantitative and three-dimensional techniques. Deflection was measured across the entire surface with high spatial resolution, allowing for comparison between regional deflection and local microstructure of the endplate and subchondral trabecular bone. Another strength of this study is that it made direct temporal connections between the observed endplate deflection and the load-carrying capacity of the vertebral body under axial compression.

After the sudden increase in endplate deflection, trabecular collapse was observed primarily in the superior third of the vertebral body (supplementary material: S4). In time-lapsed failure analyses of specimens of trabecular bone, Nazarian et al. reported that failure occurred in a localized band with surrounding portions staying relatively intact.[34] This failure pattern is similar to the local band of trabecular collapse observed in this study, just underneath the superior endplate, where bone density is low.[35] These observations further indicate that the subchondral trabecular bone is critically involved in endplate deflection and vertebral failure. The disparity between superior and inferior endplate deflection supports previous findings that superior endplates are more susceptible to failure.[36,37] The larger endplate deflection underlying the NP vs. AF may reflect regional variations in endplate thickness,[38] trabecular microstructure, and intra-discal pressure.[25] The last factor may not be dominant, given that no effect of disc grade was found; however, a larger sample size is required to provide a definitive conclusion.

The limitations of this study primarily relate to experimental procedures. First, the temporal resolution of deflection data was coarse, providing on average only 14 load increments and as few as three increments after initiation of endplate deflection. The number of increments was limited because of long scan times and the perishable nature of the tissue. Ancillary time-course experiments of five L3 vertebrae scanned repeatedly over 72 hours showed no change in attenuation of the bone tissue ($p>0.08$). In contrast, marrow attenuation decreased 27% on average over 72 hours in four of the specimens ($p<0.01$). Thus, the current protocol is sufficient for quantifying bone parameters over several days, but the prospect of increasing the duration must be evaluated with caution. Scan times could be reduced by imaging only the endplates; however, acquiring images of the entire vertebral body aids in image registration. Second, due to size constraints of the μCT scanner, the posterior elements were removed from the vertebral body prior to testing. The neural arch may act to support the posterior cortical shell, and its absence may have led to some of the posterior (as opposed to anterior) endplate failures observed here. Future studies with thoracic segments or with larger capacity μCT scanners are needed to examine how the posterior elements affect vertebral load transmission, both in axial compression and anterior bending, a loading condition that may be associated with wedge fractures. Third, static loads differ from the dynamic loading conditions experienced *in vivo*.[39] Sustained loading exudates fluid from the IVD, causing a drop in NP pressure that shifts the load distribution to the periphery.[40] However, the ultimate loads recorded in this study agree with those obtained from continuous loading of lumbar vertebral segments.[41] Prior studies of trabecular bone have also shown good correlation between mechanical properties obtained with continuous vs. step-wise loading.[42] The Fourth, QCT is less sensitive than magnetic resonance imaging[43] for characterizing the internal anatomy of the IVD; however, the QCT-based ALDI scores[33] agreed well with the assessments based on photographs and histological sections.

In spite of these limitations, the measurements obtained in this study demonstrate that progression of endplate deflection is associated with the microstructure of the endplate and the adjoining trabecular bone, and the anatomy of the adjacent IVD. Non-recoverable endplate deflection was observed when the mechanical competence of the vertebra had been compromised, while much of the vertebral body remained undeformed. These results indicate that vertebral failure initiates as endplate deflection and that additional study of the mechanisms of endplate deflection may further elucidate the pathogenesis of age-related vertebral fractures.

Supplementary Material

Refer to Web version on PubMed Central for supplementary material.

ACKNOWLEDGEMENTS

Funding was provided by National Institutes of Health R01 AR054620 and National Science Foundation BES 0521255. The authors also thank Gabriel McDonald and Sharon Roth.

REFERENCES

1. Hasserius R, Redlund-Johnell I, Mellstrom D, et al. Vertebral deformation in urban swedish men and women: Prevalence based on 797 subjects. Acta Orthop Scand. 2001; 72:273–278. [PubMed: 11480604]
2. Melton LJ 3rd, Lane AW, Cooper C, et al. Prevalence and incidence of vertebral deformities. Osteoporos Int. 1993; 3:113–119. [PubMed: 8481586]
3. O'Neill TW, Felsenberg D, Varlow J, et al. The prevalence of vertebral deformity in european men and women: The european vertebral osteoporosis study. J Bone Miner Res. 1996; 11:1010–1018. [PubMed: 8797123]
4. Jones G, Nguyen T, Sambrook PN, et al. Symptomatic fracture incidence in elderly men and women: The dubbo osteoporosis epidemiology study (does). Osteoporos Int. 1994; 4:277–282. [PubMed: 7812076]
5. Burger H, Van Daele PL, Grashuis K, et al. Vertebral deformities and functional impairment in men and women. J Bone Miner Res. 1997; 12:152–157. [PubMed: 9240738]
6. Cauley JA, Thompson DE, Ensrud KC, et al. Risk of mortality following clinical fractures. Osteoporos Int. 2000; 11:556–561. [PubMed: 11069188]
7. Fujiwara S, Kasagi F, Yamada M, Kodama K. Risk factors for hip fracture in a japanese cohort. J Bone Miner Res. 1997; 12:998–1004. [PubMed: 9199997]
8. Lindsay R, Silverman SL, Cooper C, et al. Risk of new vertebral fracture in the year following a fracture. JAMA. 2001; 285:320–323. [PubMed: 11176842]
9. Ross PD, Davis JW, Epstein RS, Wasnich RD. Pre-existing fractures and bone mass predict vertebral fracture incidence in women. Ann Intern Med. 1991; 114:919–923. [PubMed: 2024857]
10. Jiang G, Eastell R, Barrington NA, Ferrar L. Comparison of methods for the visual identification of prevalent vertebral fracture in osteoporosis. Osteoporos Int. 2004; 15:887–896. [PubMed: 15071725]
11. Ferrar L, Jiang G, Schousboe JT, et al. Algorithm-based qualitative and semiquantitative identification of prevalent vertebral fracture: Agreement between different readers, imaging modalities, and diagnostic approaches. J Bone Miner Res. 2008; 23:417–424. [PubMed: 17967136]
12. Jiang G, Luo J, Pollintine P, et al. Vertebral fractures in the elderly may not always be "osteoporotic". Bone. 2010; 47:111–116. [PubMed: 20362704]
13. Holmes AD, Hukins DW, Freemont AJ. End-plate displacement during compression of lumbar vertebra-disc-vertebra segments and the mechanism of failure. Spine. 1993; 18:128–135. [PubMed: 8434313]
14. Hardy WG, Lissner HR, Webster JE, Gurdjian ES. Repeated loading tests of the lumbar spine; a preliminary report. Surg Forum. 1958; 9:690–695. [PubMed: 13635481]
15. Perey O. Fracture of the vertebral end-plate in the lumbar spine; an experimental biochemical investigation. Acta Orthop Scand Suppl. 1957; 25:1–101. [PubMed: 13443913]
16. Rolander SD, Blair WE. Deformation and fracture of the lumbar vertebral end plate. Orthop Clin North Am. 1975; 6:75–81. [PubMed: 1113982]
17. Yoganandan N, Maiman DJ, Pintar F, et al. Microtrauma in the lumbar spine: A cause of low back pain. Neurosurgery. 1988; 23:162–168. [PubMed: 2972940]
18. Brinckmann P, Frobin W, Hierholzer E, Horst M. Deformation of the vertebral end-plate under axial loading of the spine. Spine. 1983; 8:851–856. [PubMed: 6670020]
19. Eswaran SK, Gupta A, Adams MF, Keaveny TM. Cortical and trabecular load sharing in the human vertebral body. J Bone Miner Res. 2006; 21:307–314. [PubMed: 16418787]
20. Homminga J, Van-Rietbergen B, Lochmuller EM, et al. The osteoporotic vertebral structure is well adapted to the loads of daily life, but not to infrequent "error" loads. Bone. 2004; 34:510–516. [PubMed: 15003798]
21. Keller TS, Hansson TH, Abram AC, et al. Regional variations in the compressive properties of lumbar vertebral trabeculae: Effects of disc degeneration. Spine. 1989; 14:1012–1019. [PubMed: 2781407]

22. Simpson EK, Parkinson IH, Manthey B, Fazzalari NL. Intervertebral disc disorganization is related to trabecular bone architecture in the lumbar spine. J Bone Miner Res. 2001; 16:681–687. [PubMed: 11315995]
23. Hulme PA, Boyd SK, Ferguson SJ. Regional variation in vertebral bone morphology and its contribution to vertebral fracture strength. Bone. 2007; 41:946–957. [PubMed: 17913613]
24. Thomsen JS, Ebbesen EN, Mosekilde LI. Age-related differences between thinning of horizontal and vertical trabeculae in human lumbar bone as assessed by a new computerized method. Bone. 2002; 31:136–142. [PubMed: 12110426]
25. Adams MA, McNally DS, Dolan P. 'Stress' distributions inside intervertebral discs. The effects of age and degeneration. J Bone Joint Surg Br. 1996; 78:965–972. [PubMed: 8951017]
26. Kurowski P, Kubo A. The relationship of degeneration of the intervertebral disc to mechanical loading conditions on lumbar vertebrae. Spine. 1986; 11:726–731. [PubMed: 3787344]
27. Homminga J, Weinans H, Gowin W, et al. Osteoporosis changes the amount of vertebral trabecular bone at risk of fracture but not the vertebral load distribution. Spine. 2001; 26:1555–1561. [PubMed: 11462085]
28. Fields AJ, Lee GL, Keaveny TM. Mechanisms of initial endplate failure in the human vertebral body. J Biomech. 2010; 43:3126–3131. [PubMed: 20817162]
29. Keller TS, Ziv I, Moeljanto E, Spengler DM. Interdependence of lumbar disc and subdiscal bone properties: A report of the normal and degenerated spine. J Spinal Disord. 1993; 6:106–113. [PubMed: 8504221]
30. Hussein AI, Barbone PE, Morgan EF. Digital volume correlation for study of the mechanics of whole bones. Procedia IUTAM. 2012; 4:116–125. [PubMed: 23336099]
31. Rodriguez AG, Rodriguez-Soto AE, Burghardt AJ, et al. Morphology of the human vertebral endplate. J Orthop Res. 2012; 30:280–287. [PubMed: 21812023]
32. Thompson JP, Pearce RH, Schechter MT, et al. Preliminary evaluation of a scheme for grading the gross morphology of the human intervertebral disc. Spine. 1990; 15:411–415. [PubMed: 2363069]
33. Hussein AI, Jackman TM, Morgan SR, et al. The intravertebral distribution of bone density: Correspondence to intervertebral disc health and implications for vertebral strength. Osteoporos Int. Jul 18.2013 2013 [Epub ahead of print].
34. Nazarian A, Stauber M, Zurakowski D, et al. The interaction of microstructure and volume fraction in predicting failure in cancellous bone. Bone. 2006; 39:1196–1202. [PubMed: 16920051]
35. Hussein AI, Morgan EF. The effect of intravertebral heterogeneity in microstructure on vertebral strength and failure patterns. Osteoporos Int. 2013; 24:979–989. [PubMed: 22707063]
36. Ortiz AO, Bordia R. Injury to the vertebral endplate-disk complex associated with osteoporotic vertebral compression fractures. AJNR Am J Neuroradiol. 2011; 32:115–120. [PubMed: 20801764]
37. Trout AT, Kallmes DF, Layton KF, et al. Vertebral endplate fractures: An indicator of the abnormal forces generated in the spine after vertebroplasty. J Bone Miner Res. 2006; 21:1797–1802. [PubMed: 17002575]
38. Zhao FD, Pollintine P, Hole BD, et al. Vertebral fractures usually affect the cranial endplate because it is thinner and supported by less-dense trabecular bone. Bone. 2009; 44:372–379. [PubMed: 19049912]
39. Hulme PA, Ferguson SJ, Boyd SK. Determination of vertebral endplate deformation under load using micro-computed tomography. J Biomech. 2008; 41:78–85. [PubMed: 17915227]
40. McMillan DW, Garbutt G, Adams MA. Effect of sustained loading on the water content of intervertebral discs: Implications for disc metabolism. Ann Rheum Dis. 1996; 55:880–887. [PubMed: 9014581]
41. McCubbrey DA, Cody DD, Peterson EL, et al. Static and fatigue failure properties of thoracic and lumbar vertebral bodies and their relation to regional density. J Biomech. 1995; 28:891–899. [PubMed: 7673257]
42. Nazarian A, Muller R. Time-lapsed microstructural imaging of bone failure behavior. J Biomech. 2004; 37:55–65. [PubMed: 14672568]
43. Pfirrmann CW, Metzdorf A, Zanetti M, et al. Magnetic resonance classification of lumbar intervertebral disc degeneration. Spine. 2001; 26:1873–1878. [PubMed: 11568697]

44. Leung VY, Chan WC, Hung SC, et al. Matrix remodeling during intervertebral disc growth and degeneration detected by multichromatic fast staining. J Histochem Cytochem. 2009; 57:249–256. [PubMed: 19001641]

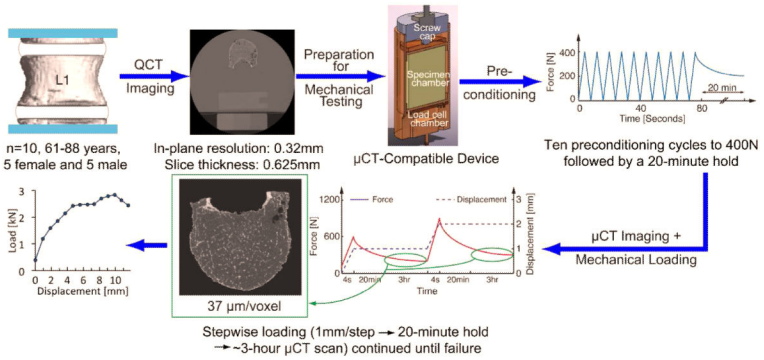

Figure 1.
Experimental procedure for mechanical testing and imaging

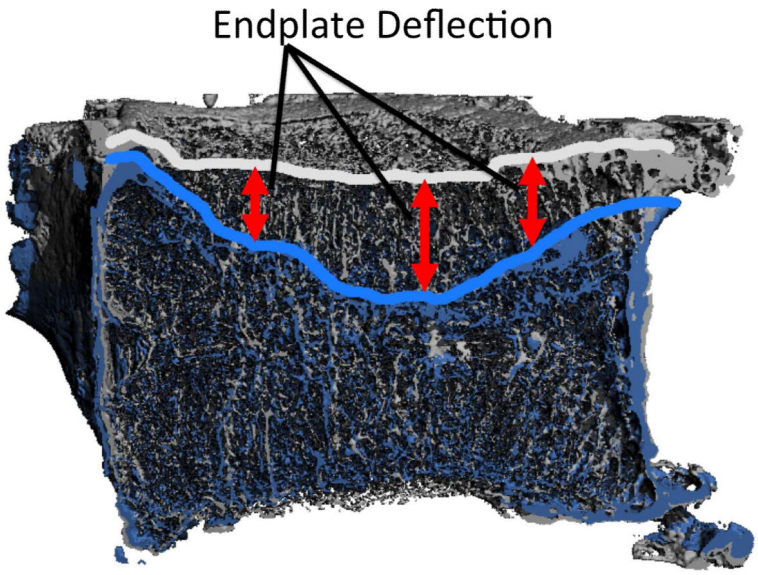

Figure 2.
Sagittal half-section of vertebra before loading (gray) and after failure (blue): Endplate deflection was defined as the vertical movement of the endplate between registered images.

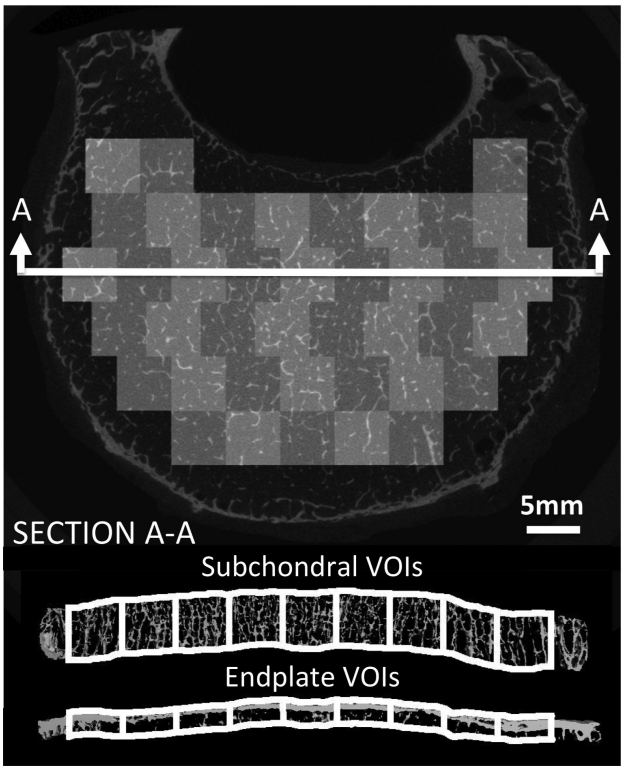

Figure 3.

Above: Transverse slice of vertebra with an overlay of the VOIs used for quantification of trabecular microstructure and Ep.BV/TV. Below: cross sectional view of the VOIs.

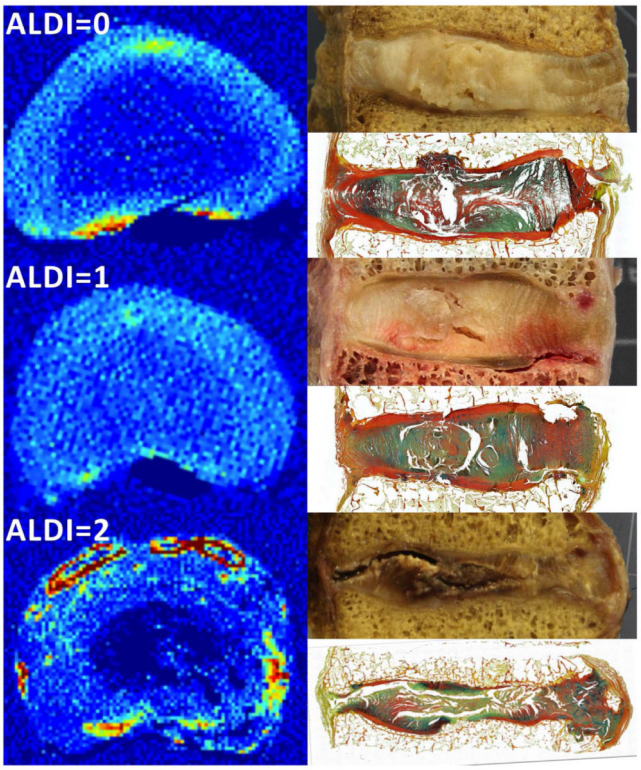

Figure 4.

ALDI scoring: Shown at the left in each of the three rows is a transverse QCT slice of the IVD (acquired prior to mechanical testing). The ALDI score is shown at the top left. Yellow, orange, and red regions are portions of the endplates and calcification within the IVD; no osteophytes were present in the QCT images of the mid-sections of these three IVDs. Shown at the top and bottom right in each row are a corresponding optical image and histological section (FAST staining[44]), respectively, of a sagittal cross-section (acquired after mechanical testing).

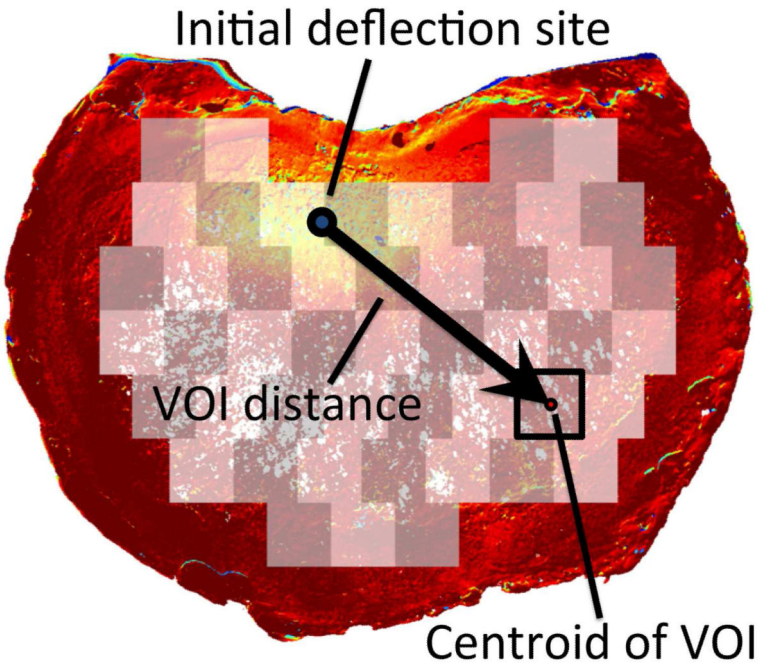

Figure 5.

VOI distance is defined as the in-plane distance from site of initial deflection to the center of a given VOI used for evaluating trabecular microstructure. Yellow indicates areas of higher endplate deflection, while red indicates areas with little or no deflection.

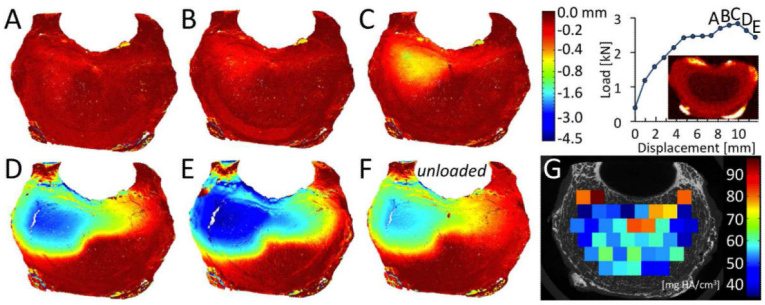

Figure 6.

(A-E) Axial deflection (negative values indicate downward movement) in the superior endplate for the six loading increments labeled on the load-displacement curve. For this vertebra, increment C is the increment of marked increase in endplate deflection. (F) Endplate deflection after unloading. (G) ρ_{app} for each VOI of subchondral trabecular bone. The deflection colorscale is non-linear, and the red image above the abscissa is the QCT image used for ALDI scoring.

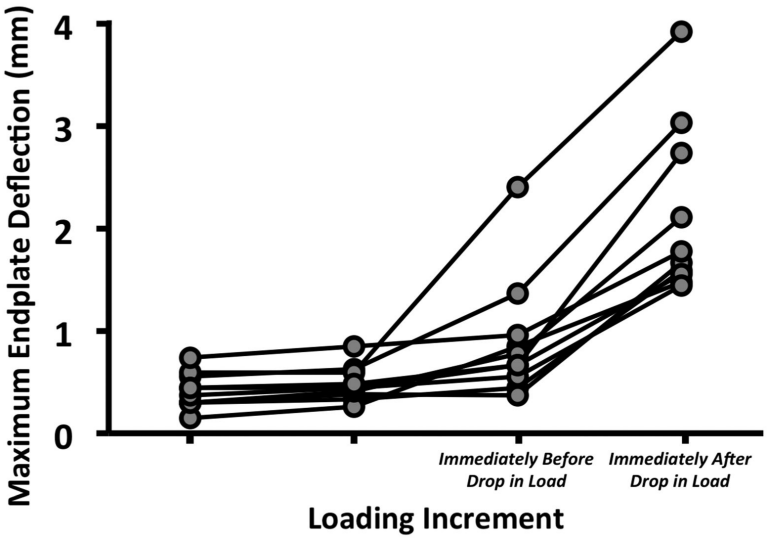

Figure 7.

Maximum endplate deflection for each specimen at loading increments leading up to and immediately after the drop in the load-displacement curve.

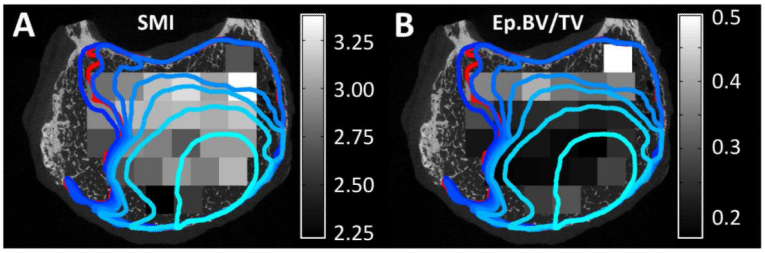

Figure 8.

Regions of large endplate deflection (outlined in blue and red), defined as >0.5 mm, and (A) distribution of SMI in the VOIs of subchondral bone (grayscale) or (B) distribution of Ep.BV/TV in the VOIs of subchondral endplate (grayscale): The lighest blue outline corresponds to the increment at which endplate deflection clearly initiated. The boundaries at subsequent increments are represented with progressively darker shades of blue. The red outline corresponds to the unloaded scan. SMI values typically range from 1 (plate-like trabeculae) to 3 (rod-like trabeculae) and can include values up to 4 (sphere-like trabeculae).

Table 1

Ultimate force (in N) and the drop in force occurring after the ultimate point (in N and as a percentage of the ultimate force): values presented are mean ± standard deviation (SD), minimum and maximum for the 10 specimens.

		Mean ± SD	Min.	Max.
Ultimate Force (N)		2,184 ± 702	1,138	3,055
Drop in Force Following Ultimate Point	N %	196 ± 92 (11.0 ± 8.3)	71 (2.9)	329 (28.9)

Table 2

Maximum endplate deflection measured before and after the load drop and increase in deflection between these two load increments, expressed in mm and as a percentage of the height of the vertebral body: values presented are mean ± standard deviation (SD), minimum and maximum for the 10 specimens.

	Mean ± SD (mm) (%)	**Min. (mm) (%)**	**Max. (mm) (%)**
Maximum Deflection at Ultimate Point	0.91 ± 0.60 (3.7 ± 2.7)	0.37 (1.6)	2.41 (10.7)
Maximum Deflection at After Load Drop	2.13 ± 0.83 (8.6 ± 3.7)	1.44 (5.2)	3.92 (17.5)
Increase in Deflection	1.22 ± 0.44 (4.9 ± 1.8)	0.63 (2.2)	2.07 (7.6)